Journal of Power Sources 208 (2012) 153–158

Contents lists available at SciVerse ScienceDirect

Journal of Power Sources

journal homepage: www.elsevier.com/locate/jpowsour

Optimized energy conversion efficiency in solid-oxide fuel cells implementing $SrMo_{1-x}Fe_xO_{3-\delta}$ perovskites as anodes

R. Martínez-Coronado[a], J.A. Alonso[a,*], A. Aguadero[a,b], M.T. Fernández-Díaz[c]

[a] Instituto de Ciencia de Materiales de Madrid, C.S.I.C., Cantoblanco, E-28049 Madrid, Spain
[b] Department of Materials, Imperial College London, London SW7 2AZ, United Kingdom
[c] Institut Laue Langevin, BP 156X, Grenoble F-38042, France

ARTICLE INFO

Article history:
Received 2 November 2011
Received in revised form 27 January 2012
Accepted 1 February 2012
Available online 9 February 2012

Keywords:
IT-SOFC
Anode
Perovskite
$SrMoO_3$

ABSTRACT

Oxides of composition $SrMo_{1-x}Fe_xO_{3-\delta}$ ($x = 0.1$, 0.2) have been prepared, characterized and tested as anode materials in single solid-oxide fuel cells, yielding output powers close to 900 mW cm^{-2} at 850 °C with pure H_2 as a fuel. This excellent performance is accounted for the results of an "in situ" neutron powder diffraction experiment, at the working temperature of the SOFC, showing the presence of a sufficiently high oxygen deficiency, with large displacement factors for oxygen atoms that suggest a large lability and mobility, combined with a huge metal-like electronic conductivity, as high as 340 S cm^{-1} at $T = 50$ °C for $x = 0.1$. The magnitude of the electronic conductivity decreases with increasing Fe-doping content. An adequate thermal expansion coefficient, reversibility upon cycling in oxidizing–reducing atmospheres and chemical compatibility with the electrolyte make these oxides good candidates for anodes in intermediate-temperature SOFC (IT-SOFCs).

1. Introduction

Fuel cells are clean and efficient electrochemical devices where the chemical energy of a fuel (fossil resources and derivatives such as hydrogen, alcohols, etc.) is directly converted into electrical energy. High-temperature fuel cells exhibit higher efficiency and are less sensitive to fuel impurities than fuel cells working at low temperatures, so the former can operate under a wide variety of fuels (e.g. hydrogen, methane, carbon monoxide, naphta, gas oil, kerosene, gas oil, gases of biomass and landfill wastes). Among the high-temperature fuel cells, Solid Oxide Fuel Cells (SOFCs) are advantageous because they are constituted by solid materials. As a drawback, the conditions undergone by the components of the SOFCs working at temperatures of typically 1000 °C are extremely demanding, which leads to too short working lives and expensive maintenance. Therefore, the reduction of the operating temperature to the 500–850 °C range keeping a high performance (durability, power output, etc.) values is one of the major requirements for a viable commercialization of these devices. The development of mixed ionic-electronic conductors (MIECs) as electrodes with the adequate performance is one of the challenges to reduce the SOFC operating temperature without detrimental of the cell efficiency [1]. In this sense many efforts have been conducted towards the development of new oxide materials of transition metals with the suitable properties.

The rate-limiting step of this electrochemical conversion is the fuel-oxidation reaction at the anode. The conventional Ni-YSZ (yttria-stabilized zirconia) or Ni-LDC (lanthanum-doped ceria) cermets catalyze the carbon formation during direct oxidation of hydrocarbon fuels and suffer from sintering problems during the cell operation [2–4]. Moreover, Ni- based anodes are susceptible to sulfur poisoning [5], whereas copper–ceria cermets (Cu–CeO_2) lacks of the adequate thermal stability. The development of MIEC oxides stable under reducing atmosphere is one important topic under investigation. Several works have demonstrated a great performance of Mo-based double perovskites operating in H_2 or CH_4 as a fuel [6–9]. $AMoO_3$ (A = Ca, Sr, Ba) perovskites, nominally containing Mo^{4+} cations, have adequate electron transfer energies as to screen and cancel the electrostatic energy accompanied by the electron transfer.

The $SrMoO_3$ cubic perovskite (containing Mo(IV) at the B-sites of the ABO_3 perovskite structure) has been reported to present one of the highest electrical conductivity values at room temperature for a ceramic material ($\sim 10^4$ S cm^{-1}) [10]; however this oxygen-stoichiometric oxide cannot exhibit the required oxygen-ion diffusion and conductivity. Whilst oxides containing Mo(IV) generally need to be synthesized in a reducing atmosphere to avoid the formation of the more stable Mo(VI) (d^0) configuration, the fascinating properties of even simple oxides such as MoO_2 [11] and $Ln_2Mo_2O_7$ [12] more than justify the synthetic effort. Moreover, from these studies it is evident that the magnetic properties

* Corresponding author. Tel.: +34 91 334 9071; fax: +34 91 372 0623.
E-mail address: ja.alonso@icmm.csic.es (J.A. Alonso).

0378-7753/$ – see front matter © 2012 Elsevier B.V. All rights reserved.
doi:10.1016/j.jpowsour.2012.02.002

of $SrMoO_3$ are much more influenced by substitution at the Mo site than the Sr sites due to the crucial role of Mo ions in $SrMoO_3$ materials [13]. Nevertheless, by suitably doping this material with trivalent elements at the B-site we demonstrate it is possible to induce the necessary oxygen vacancies in $SrMo_{1-x}Fe_xO_{3-\delta}$, in order to exhibit the adequate mixed ionic-electronic conductivity.

In this work, we show that the mentioned materials can be successfully used as anodes in SOFCs with H_2 as a fuel, with a boosted efficiency with respect to conventional cermets or double-perovskite oxides. For this purpose, single cells have been set up and tested using $SrMo_{1-x}Fe_xO_{3-\delta}$ (SMFO, $x = 0.1$, 0.2) as anode, $SrCo_{0.8}Fe_{0.2}O_{3-\delta}$ (SCFO) as cathode and $La_{0.8}Sr_{0.2}Ga_{0.83}Mg_{0.17}O_{3-\delta}$ (LSGM) as electrolyte. We report on the results of a complete characterization study including the electrical performance of the single cell, dilatometry, conductivity, chemical compatibility, redox reversibility and the structural characterization from NPD data, which is a powerful tool [14] to examine, in situ, the material under the usual conditions of a SOFC (under low pO_2 atmosphere for the anode).

2. Experimental

$SrMo_{1-x}Fe_xO_3$ ($x = 0.1$, 0.2) polycrystalline powders were prepared by soft-chemistry procedures. Stoichiometric amounts of $Sr(NO_3)_2$, $(NH_4)_6Mo_7O_{24}{\cdot}4H_2O$ and $C_2FeO_4{\cdot}2H_2O$ were solved in citric acid and some drops of nitric acid. The solution was then slowly evaporated, leading to organic resins that contain a homogeneous distribution of the involved cations. The formed resins were dried at 120 °C and decomposed at 600 °C for 12 h in order to eliminate the organic materials and the nitrates. A final treatment at 1050 °C in a tubular furnace under a $H_2(5\%)/N_2$ flow for 15 h led to the formation of the wanted perovskite oxides. Subsequent treatments at higher temperatures (1150 °C) in $5\%H_2$ demonstrate that the obtained perovskites are stable and not led to the formation of secondary phases.

The initial characterization of the product was carried out by XRD with a Bruker-axs D8 Advanced diffractometer (40 kV, 30 mA), controlled by a DIFFRACT^{PLUS} software, in Bragg–Brentano reflection geometry with Cu Kα radiation ($\lambda = 1.5418$ Å) and a PSD (Position Sensitive Detector). A filter of nickel allows the complete removal of Cu Kβ radiation. The slit system was selected to ensure that the X-ray beam was completely within the sample for all 2θ angles. For the structural refinement NPD patterns were collected at the D2B diffractometer of the Institut Laue-Langevin, Grenoble, with a wavelength $\lambda = 1.594$ Å, at 22, 250, 500, 750 and 850 °C for $x = 0.2$ and 22 °C for $x = 0.1$. About 2 g of the sample were contained in a vanadium can and placed in the isothermal zone of a furnace with a vanadium resistor operating under vacuum ($P_{O_2} \approx 10^{-6}$ Torr), and the counting time was 2 h per pattern in the high-intensity mode. The NPD data were analyzed by the Rietveld method [15] with the FULLPROF program [16]. A pseudo-Voigt function was chosen to generate the line shape of the diffraction peaks. The following parameters were refined in the final run: scale factor, background coefficients, zero-point error, pseudo-Voigt corrected for asymmetry parameters, positional coordinates and isotropic thermal factors for all the atoms. The coherent scattering lengths for Sr, Fe, Mo, and O were 7.02, 9.45, 6.72, and 5.803 fm, respectively [16].

Thermal analysis was carried out in a Mettler TA3000 system equipped with a TC10 processor unit. Thermogravimetric (TG) curves were obtained in a TG50 unit, working at a heating rate of 10 °C min^{-1}, in a O_2 flow of 0.3 L min^{-1} using about 50 mg of sample in each experiment.

Measurements of the thermal expansion coefficient and electrical conductivity required the use of sintered samples. The obtained density is around 90–95%. Thermal expansion of the sintered samples was performed in a dilatometer Linseis L75HX1000, between 300 and 900 °C in $H_2(5\%)/N_2(95\%)$. The conductivity was measured between 25 and 850 °C in $H_2(5\%)/N_2(95\%)$, by the four-point method in bar-shaped pellets under DC currents between 0.1 and 0.5 A. The currents were applied and collected with a Potenciostat-Galvanostat AUTOLAB PGSTAT 302 from ECO CHEMIE.

Single cell tests were carried out using LSGM pellets as electrolyte, $SrCo_{0.8}Fe_{0.2}O_3$ (SCFO) as cathode material, and $SrMo_{1-x}Fe_xO_3$ (SMFO) as anode material. The LSGM pellets of 20-mm diameter were sintered at 1450 °C for 20 h and then polished with a diamond wheel to a thickness of 300 μm. $La_{0.4}Ce_{0.6}O_{2-\delta}$ (LDC) was used as a buffer layer between the anode and the electrolyte in order to prevent the interdiffusion of ionic species. Inks of LDC, SMFO and SCFO were prepared with a binder (V-006 from Heraeus). LDC ink was screen-printed onto one side of the LSGM disk followed by a thermal treatment at 1300 °C in air for 1 h. SMFO was subsequently screen printed onto the LDC layer and fired at 1100 °C in air for 1 h. SCFO was finally screen printed onto the other side of the disk and fired at 1100 °C in air for 1 h. The working electrode area of the cell was 0.24 cm^2 (0.6 cm × 0.4 cm). Pt gauze with a small amount of Pt paste in separate dots was used as current collector at both the anodic and the cathodic sides for ensuring electrical contact. The cells were tested in a vertical tubular furnace at 750, 800 and 850 °C; the anode side was fed with pure H_2, with a flow of 20 ml min^{-1}, whereas the cathode worked in an air flow of 100 ml min^{-1}. The fuel-cell tests were performed with an AUTOLAB 302N Potentiostat/Galvanostat by changing the voltage of the cell from 1.2 to 0.1 V, with steps of 0.010 V, holding 10 s at each step. Current density was calculated by the recorded current flux through the effective area of the cell (0.24 cm^2). Each *VI* (voltage–intensity) scan corresponds to one cycle; the activation of the cell was followed in subsequent cycles until the full power of the single cell was reached.

3. Results and discussion

3.1. Crystallographic characterization

$SrMo_{1-x}Fe_xO_3$ ($x = 0.1$, 0.2) samples were obtained as black-reddish, well-crystallized powders. Single-phase cubic perovskite phases were identified from laboratory XRD (Fig. 1), $a = 3.9605(2)$ and 3.9542(1) Å for $x = 0.1$ and 0.2, respectively. No impurity phases were detected. A neutron powder diffraction (NPD) study at room temperature (RT) and high temperature for the Fe-doped samples

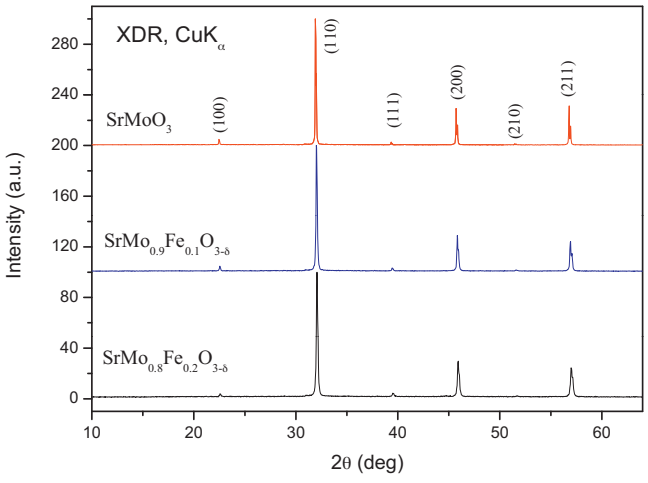

Fig. 1. XRD patterns with Cu Kα radiation for $SrMoO_3$ and $SrMo_{1-x}Fe_xO_{3-\delta}$ ($x = 0.1$, 0.2), characteristic of pure cubic perovskite phases.

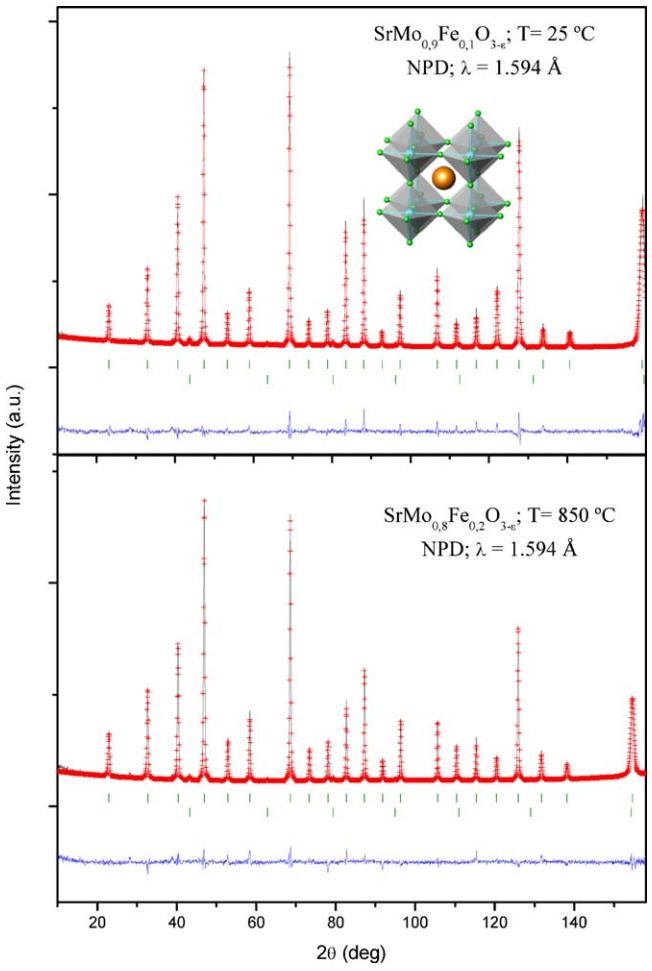

Fig. 2. Observed (crosses), calculated (full line) and difference (at the bottom) NPD profiles for $SrMo_{0.9}Fe_{0.1}O_{3-\delta}$ at 295 K and for $SrMo_{0.8}Fe_{0.2}O_{3-\delta}$ at 1123 K in vacuum ($P_{O_2} = 10^{-6}$ Torr), refined in the cubic $Pm\bar{3}m$ space group. The vertical markers correspond to the allowed Bragg reflections. The second series of Bragg reflections correspond to vanadium from the sample holder.

was useful to investigate the structural details in relation with the performance of these materials as anodes. The crystal structure was defined in the $Pm\bar{3}m$ space group (no. 225), $Z = 1$. Sr atoms are located at 1b (1/2,1/2,1/2) positions, Mo and Fe distributed at random at 1a (0,0,0), and oxygen atoms O at 3d (1/2,0,0). The occupancy factors of oxygen atoms were also refined in the final run; a negligible oxygen deficiency is observed at RT. Fig. 2a illustrates the good agreement between the observed and calculated NPD patterns for $SrMo_{0.9}Fe_{0.1}O_3$ at RT. The inset of Fig. 2a illustrates the cubic perovskite unit cell.

Table 1 summarizes the unit-cell, atomic, thermal parameters, discrepancy factors and interatomic distances after the Rietveld refinements of the doped samples at room temperature. The lattice parameters decrease with the increasing Fe-doping level x. At RT the ⟨Mo,Fe–O⟩ bond lengths become progressively smaller (1.9802(2) and 1.9771(1) Å for $x = 0.1$ and 0.2, respectively) with respect to those given for the parent $SrMoO_3$ perovskite [17], of 1.9881(1) Å, even if the ionic size of high-spin Fe^{3+} (0.645 Å) is virtually the same as Mo(IV) (0.65 Å) [18]. This fact may indicate that the oxidation state of Mo steadily increases with doping, giving rise to a mixed-valence state Mo(IV)–Mo(V) proportional to the doping rate. The aristotype (simple-cubic sub-cell) of the double-perovskite Sr_2MoFeO_6, has a lattice parameter of 3.942 Å [19], also indicating the tendency of the lattice parameter to decrease with Fe-doping

Table 1
Unit-cell and thermal parameters for $SrMo_{1-x}Fe_xO_3$ ($x = 0.1$ and 0.2) in cubic $Pm\bar{3}m$ (no. 221) space group, from NPD at 295 K. Sr is placed at 1b (1/2,1/2,1/2), (Mo,Fe) at 1a (0,0,0) and O1 at 3d (1/2,0,0) position.

D2B (RT)	$SrMoO_3$[a]	$SrMo_{0.9}Fe_{0.1}O_3$	$SrMo_{0.8}Fe_{0.2}O_3$
a (Å)	3.97629(3)	3.9605(5)	3.9542(3)
V (Å^3)	62.869(7)	62.125(1)	61.828(1)
Sr 1b (1/2,1/2,1/2)			
B_{iso}	0.77(3)	1.047(4)	1.037(2)
f_{occ}	1.000	1.000	1.000
Mo/Fe 1a (0,0,0)			
B_{iso}	0.55(4)	0.460(3)	0.284(2)
Mo/Fe f_{occ}	1.000	0.940(1)/0.06(1)	0.855(1)/0.145(2)
O1 3d (1/2,0,0)			
B_{iso}	0.75(10)	1.018(2)	0.965(1)
f_{occ}	1.000	0.996(2)	0.997(1)
Reliability factors			
χ^2	–	4.32	7.03
R_p (%)	–	4.70	3.53
R_{wp} (%)	–	5.68	4.29
R_{exp} (%)	–	3.34	1.88
R_I (%)	–	4.02	4.92
Distances (Å)			
(Sr)–(O1)	–	2.8005(2)	2.7960(2)
(Mo/Fe)–(O1)	1.98814(1)	1.9802(2)	1.9771(3)

[a] Taken from Ref. [18].

the Mo site. The result is a redox balance between Mo(IV)–Mo(V) and Fe^{3+}, since the oxygen sublattice seems not to be affected.

Secondly, the thermal evolution of the crystal structure under the anode conditions in a SOFC was evaluated by NPD for $x = 0.2$. For this purpose, the samples were contained in a vanadium can under high vacuum (10^{-6} Torr) and the NPD data were collected in situ in a furnace at 250, 550, 750 and 850 °C. The NPD data, illustrated in Fig. 3, show no structural transition along the temperature range under study (25–850 °C). Good agreement factors were reached at the different temperatures for the mentioned simple-perovskite structural model; for instance $R_p = 4.33\%$, $R_{wp} = 5.60\%$, $\chi^2 = 2.89$ and $R_I = 6.47\%$ at $T = 850$ °C for $x = 0.2$; the goodness of this fit is illustrated in Fig. 2b. Table 2 summarizes the results obtained from the refinements at the different temperatures for $SrMo_{0.8}Fe_{0.2}O_3$.

The thermal evolution of the oxygen content in air was also studied by NPD. Fig. 4 illustrates the temperature dependence of the concentration of oxygen vacancies (δ) and unit-cell parameters for $SrMo_{0.8}Fe_{0.2}O_{3-\delta}$. The oxygen content decreases when heating the sample in vacuum from $SrMo_{0.8}Fe_{0.2}O_{2.992(9)}$ at RT to a highly reduced $SrMo_{0.8}Fe_{0.2}O_{2.952(9)}$ at 850 °C. This fact suggest that the mixed-valence Mo(IV)–Mo(V) becomes reduced to Mo(IV) upon

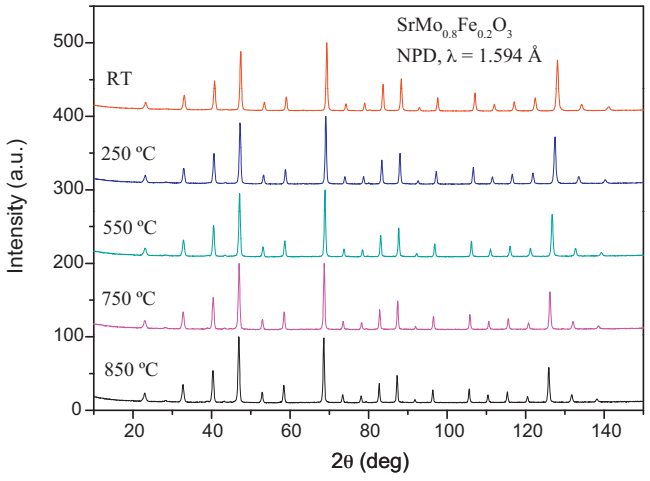

Fig. 3. Thermal evolution of the NPD patterns for $SrMo_{0.8}Fe_{0.2}O_3$ between RT and 850 °C.

Table 2
Unit-cell, thermal parameters and selected distances (Å) for $SrMo_{0.8}Fe_{0.2}O_3$ in cubic $Pm\bar{3}m$ (no. 221) space group, from NPD at RT to 850 °C.

$SrMo_{0.8}Fe_{0.2}O_3$	RT	250	550	750	850
a (Å)	3.9542(3)	3.9641 (3)	3.9772(5)	3.9871(7)	3.9922(6)
V (Å^3)	61.828(1)	62.291(1)	62.911(1)	63.381(2)	63.625(2)
Sr 1b (1/2,1/2,1/2)					
B_{iso}	1.037(2)	1.495(4)	2.059(4)	2.506(5)	2.728(5)
f_{occ}	1.000	1.000	1.000	1.000	1.000
Mo/Fe 1a (0,0,0)					
B_{iso}	0.284(2)	0.501(3)	0.610(3)	0.905(4)	1.026(4)
Mo/Fe f_{occ}	0.855/0.145	0.855/0.145	0.855/0.145	0.855/0.145	0.855/0.145
O1 3d (1/2,0,0)					
B_{iso}	0.965(1)	1.314(2)	1.871(3)	2.315(3)	2.582(4)
f_{occ}	0.997(1)	0.993(2)	0.990(1)	0.987(3)	0.984(9)
Reliability factors					
χ^2	7.03	3.97	4.41	5.07	4.56
R_p (%)	3.53	4.50	4.49	4.82	4.33
R_{wp} (%)	4.29	5.29	5.62	6.19	5.60
R_{exp} (%)	1.88	3.32	3.32	3.33	3.29
R_I (%)	4.92	6.06	6.64	6.64	6.47
Distances (Å)					
(Sr)–(O1)	2.7960(2)	2.8030(2)	2.8123(3)	2.8193(4)	2.8229(3)
(Mo/Fe)–(O1)	1.9771(3)	1.9820(2)	1.9886(3)	1.9935(4)	1.9961(3)

heating, generating oxygen vacancies. These vacancies are essential to drive the required O^{2-} motion in a MIEC oxide. Moreover, the isotropic displacement factors (B) of the oxygen atoms increase from 0.965(1) Å^2 (22 °C) to 2.582(4) Å^2 (850 °C), as shown in Fig. 4b, indicating a high mobility or chemical lability of these oxygen atoms, thus suggesting a high ionic conductivity at the working temperatures of the SOFC.

3.2. Thermal analysis (TGA)

The thermal evolution of the samples was studied by recording TGA curves. Heating $SrMo_{1-x}Fe_xO_{3-\delta}$ ($x = 0.2$) in O_2 flow leads to the oxidation of this material to give $SrMo_{1-x}Fe_xO_{3.67}$ ($x = 0.2$) with a scheelite-type crystal structure. Fig. 5 shows the thermal analysis curve obtained in O_2, displaying the incorporation of 0.67 oxygen atoms in the 400–500 °C temperature range, and the inset displays the refined XRD pattern of the oxygen-defective scheelite phase (space group $I4_1/a$ (no. 88)). A thermal treatment of the resulting scheelite phase in reducing (H_2(5%)/N_2) atmosphere restores the perovskite phase, thus confirming the required reversibility upon cycling in oxidizing–reducing atmospheres.

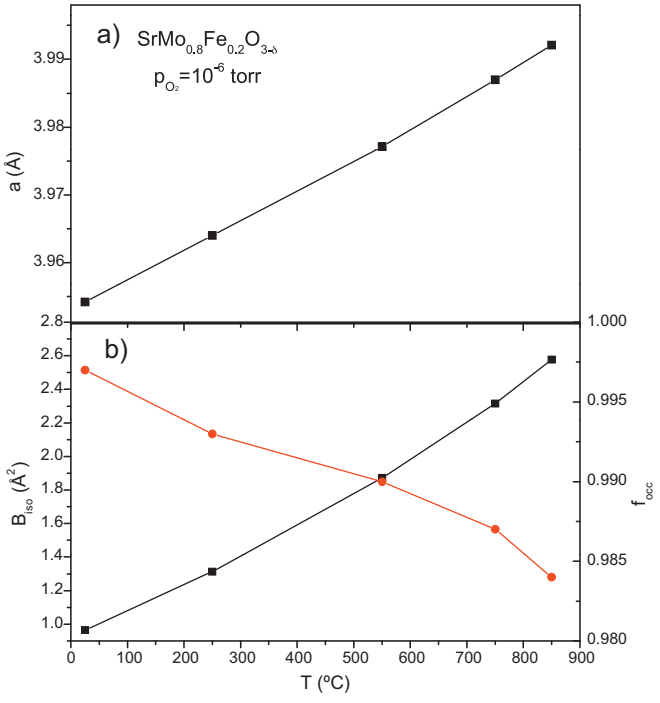

Fig. 4. Thermal variation of (a) unit-cell parameter and (b) isotropic displacement factor for O atoms (left axis) and oxygen occupancy factor (right axis), from in situ NPD data.

3.3. Thermal expansion measurements and chemical compatibility

Aiming to determine the mechanical compatibility of our anode material with the other cell components, thermal expansion measurement of the dense ceramic was carried out in a 5%H_2 atmosphere. The thermal expansion of each perovskite phase was measured in sintered pellets, first preheated in air at 950 °C for 12 h and finally reduced in a 5%H_2 flow at 900 °C for 15 h. A dilatometric analysis was performed between 35 and 850 °C for several cycles; the data where only recorded during the heating runs. Fig. 6 shows no abrupt changes in the thermal expansion

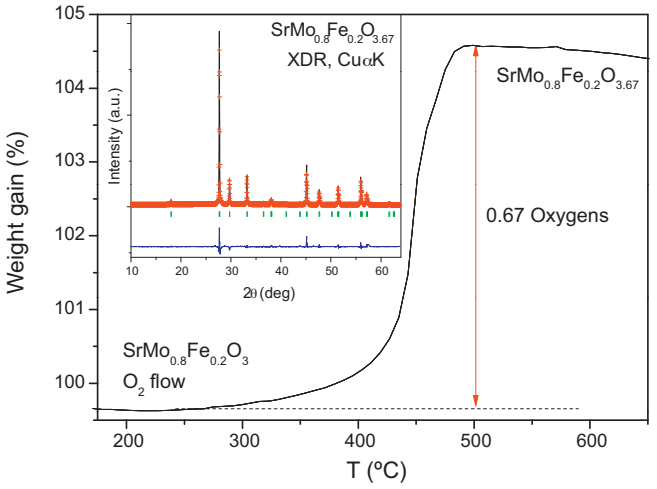

Fig. 5. Thermal analysis in O_2 flow (TG curve) of $SrMo_{0.8}Fe_{0.2}O_{3-\delta}$ perovskite, showing an oxidation step to a scheelite phase; the inset displays the Rietveld plot after the structural refinement from XRD data of the oxidation product. Crystal data for $SrMo_{0.8}Fe_{0.2}O_{3.7}$ scheelite: $a = b = 5.3960(3)$ Å, $c = 12.0336$ Å; space group $I4_1/a$ (no. 88), $Z = 4$. Sr at 4b (0,1/4,5/8); Mo/Fe at 4a (0,1/4,1/8), O at 16f (0.2479(3),0.1200(2),0.0541(3)) sites.

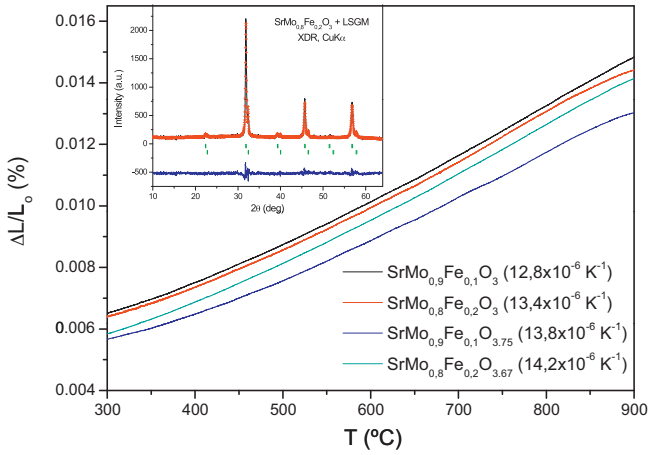

Fig. 6. Thermal expansion determined by dilatometry of the $SrMo_{1-x}Fe_xO_3$ and $SrMo_{1-x}Fe_xO_{4-\delta}$ series. The inset shows the Rietveld-refined XRD profiles of a mixture of LSGM and $SrMo_{0.8}Fe_{0.2}O_{3-\delta}$ after a thermal treatment at 900 °C in H_2(5%)/N_2, showing no reaction products between both phases other than the initial reactants. The first and second series of Bragg positions correspond to LSGM and $SrMo_{0.8}Fe_{0.2}O_{3-\delta}$, respectively.

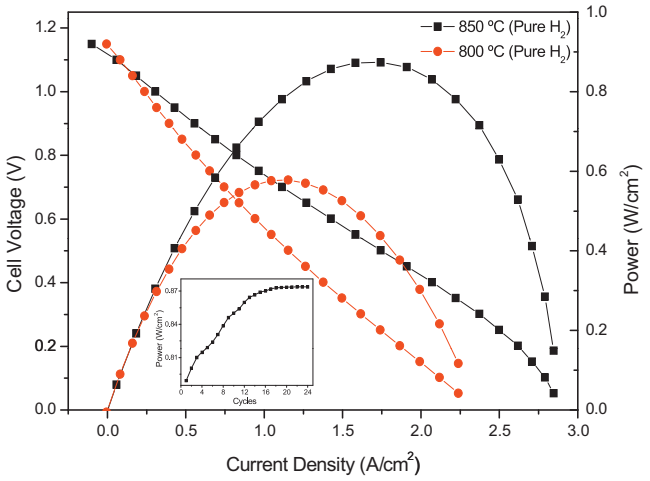

Fig. 8. Cell voltage (left axis) and power density (right axis) as a function of the current density for the test cell with the configuration SMFO(x = 0.1)/LDC/LSGM/SCFO in pure H_2 measured at T = 750, 800 and 850 °C. The inset shows the evolution of the power density as a function of the number of cycles at 850 °C.

of $SrMo_{1-x}Fe_xO_{3-\delta}$ in all the temperature range under measurement. The TEC measured under 5% H_2/95% N_2 atmosphere between 300 and 850 °C is 12.8×10^{-6} K^{-1} and 13.4×10^{-6} K^{-1} for x = 0.1 and 0.2, respectively; this value is in good agreement with that obtained from neutron diffraction data in the heating run, of 11.61×10^{-6} K^{-1}. Moreover, the thermal expansion of the oxygen-defective scheelite phase (x = 0.1) shows a value of 13.8×10^{-6} K^{-1} when heating the sample between 300 and 850 °C in air, very similar to that obtained for the reduced perovskite and that perfectly matches with the values usually displayed by SOFC electrolytes. This behavior is also verified in the sample x = 0.2.

The chemical compatibility of $SrMo_{1-x}Fe_xO_{3-\delta}$ with the LSGM electrolyte has also been checked by firing mixtures of both powdered materials at 900 °C in H_2(5%)/N_2(95%) for 24 h; the inset of Fig. 6 shows a Rietveld analysis of the product, consisting in a mixture of both unaltered perovskite phases.

3.4. Electrical conductivity measurements

Fig. 7 shows the thermal variation of the electrical conductivity of $SrMo_{1-x}Fe_xO_{3-\delta}$ (x = 0.1, 0.2) measured in sintered bars in 5% H_2/95% N_2 atmosphere by the *dc* four-probe method. A current load

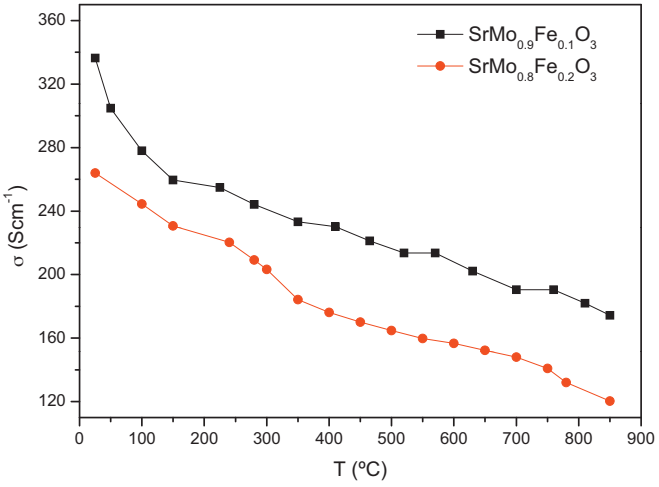

Fig. 7. *dc*-conductivity as a function of temperature for $SrMo_{1-x}Fe_xO_{3-\delta}$ (x = 0.1, 0.2).

of 100 mA was applied and the potential drop was recorded in an AUTOLAB 302N Potentiostat-Galvanostat. The perovskite materials show a metallic-like conductivity under reducing conditions; for instance for x = 0.2, σ = 265 S cm^{-1} at 50 °C and 120 S cm^{-1} at 850 °C; these values are even higher for x = 0.1, σ = 305 S cm^{-1} at 50 °C and 175 S cm^{-1} at 850 °C. There is a clear decrease in the electrical conductivity when the Fe content increases, since Fe^{3+} disrupts the conduction paths via Mo(IV)–O–Mo(IV) chemical bonds. As expected, when the perovskite phase is oxidized to the scheelite structure it becomes an insulator.

3.5. Fuel-cell tests

The performance of $SrMo_{1-x}Fe_xO_{3-\delta}$ as anode was tested in single cells in an electrolyte-supported configuration using a 300-μm-thick LSGM electrolyte. Fig. 8 illustrates the cell voltage and power density as a function of current density at 800 and 850 °C for the single cells fed with pure H_2 for the x = 0.1 anode. The maximum power densities generated by the cell are 578 and 874 mW cm^{-2}, respectively. The inset of Fig. 8 shows the maximum power density of the single cell as a function of the number of cycles. The output power increases during the first 20 cycles as the anode is becoming totally reduced by the fuel; this process corresponds to the activation of the cell. After 20 cycles the power density remains stable at the mentioned maximum, 874 mW cm^{-2}.

Fig. 9 illustrates the cell voltage and power density as a function of current density at 750, 800 and 850 °C for the single cells fed with pure H_2 for the x = 0.2 anode. The maximum power densities generated by the cell are 336, 551 and 790 mW cm^{-2}, respectively. A view of the cathodic side of the single cell is included as an inset in Fig. 9. Although both anodes perform well, a slight decrease of the out power of the single cells is observed for x = 0.2 with respect to x = 0.1 anode. This reduction of the power density could related to the decrease in the Mo contents of the anode in the x = 0.2 sample, since apparently molybdenum is responsible for the catalytic oxidation of the fuel, as it has been observed in other Mo-containing anodes [6]. In spite of the more important number of oxygen vacancies supposed to be introduced into the x = 0.2 oxide upon Fe doping, the x = 0.1 sample seems to exhibit a good compromise between both determining factors, the catalytic activity and the ionic conductivity.

In order to compare the performance of our $SrMo_{1-x}Fe_xO_{3-\delta}$ anodes with the usual Ni cermets, an identical single cell with

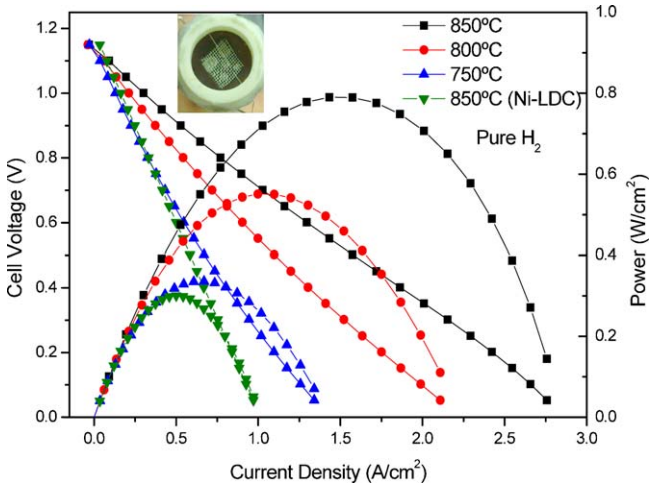

Fig. 9. Cell voltage (left axis) and power density (right axis) as a function of the current density for the test cell with the configuration SMFO(x = 0.2)/LDC/LSGM/SCFO in pure H_2. The performance at 850 °C is compared to that of the standard Ni-LDC cermet anode; a loss of more than 50% of the power density is observed. The inset shows a view of the cathodic side of the single cell.

Ni–$Ce_{0.8}La_{0.2}O_{2-\delta}$ (LDC) cermet as the anode was also built and evaluated. It is important to note that with LSGM electrolyte the reaction between the electrolyte and Ni may occur due to the diffusion of Ni into LSGM leading to the formation of a highly resistive phase resulting in the degradation of the cell performance [20,21]. Some authors observed that the use of a buffer layers such as the La-doped ceria (LDC) helps to minimize the reaction between Ni and LSGM improving the performance of the cell [22,23]. On the other hand, Zhang et al. evidenced that the sintering temperature of a Ni ceria cermet anode on a LSGM electrolyte is determinant on the reactivity between both species finding that the anode sintered at 1250 °C displays minimum anode polarization suggesting this sintering temperature as the optimum to deposit Ni-ceria cermets on LSGM electrolyte [24]. Those conditions were used to deposit and sinter the cermet on the anodic side of our single cell. Fig. 9 includes the power density obtained at 850 °C for the standard cermet Ni-LDC; a much inferior power output is observed in this case with respect to the $SrMo_{1-x}Fe_xO_{3-\delta}$ anodes. In fact, Fig. 9 shows a loss of more than 50% of the power density when using the cermet anode at 850 °C, decreasing from 790 to 300 mW cm^{-2}.

4. Conclusion

In summary, we have shown that $SrMo_{1-x}Fe_xO_{3-\delta}$ oxides can be successfully utilized as anode materials in single SOFC cells with LSGM as electrolyte. A maximum power density of 870 and 790 mW cm^{-2} was obtained at 850 °C with pure H_2 as fuel for x = 0.1 and 0.2, respectively. We can correlate the good performance observed in the single-cell tests with the structural features obtained from NPD data collected in the usual working conditions of an anode (low pO_2) in a SOFC. The crystal structure has been refined at RT in the cubic $Pm\bar{3}m$ space group, and no structural transitions have been observed in the investigated temperature interval (25–850 °C). The sufficiently large number of oxygen vacancies together with high isotropic thermal factors suggest a high ionic conductivity. The extraordinary performance of the anode material relies on the association of the high electronic conductivity derived from the parent $SrMoO_3$ compound and the oxygen vacancies induced upon Fe doping, providing the suitable ionic transport; the result is an excellent catalyst for hydrogen oxidation. The electrical characterization evidences a metallic behavior in these perovskites. The thermal expansion coefficient was between 12.8×10^{-6} and 13.4×10^{-6} K^{-1}, very close to those of the usual SOFC electrolytes at these temperatures. The reversibility of the reduction-oxidation between the $Sr(Mo,Fe)O_{4-\delta}$ scheelite and $Sr(Mo,Fe)O_3$ perovskite phases makes it possible the required cyclability of the cells. This perovskite-scheelite phase transition is totally reversible and it is not expected to lead to cracking problems during the cell operation.

Acknowledgements

We acknowledge the financial support of the Spanish "Ministerio de Ciencia e Innovación" (MICINN) to the project MAT2010-16404. We are grateful to ILL for making the beamtime available. A.A. also thanks to MICINN for a "Juan de la Cierva" contract and a "Jose Castillejo" Fellowship.

References

[1] S.B. Adler, Chem. Rev. 104 (2004) 4791–4843.
[2] S.P. Jiang, S.H. Chan, Mater. Sci. Technol. 20 (2004) 1109.
[3] B.C.H. Steele, I. Kelly, M. Middleton, R. Rudkin, Solid State Ionics 28–30 (1988) 1547.
[4] Y. Matsuzaki, I. Yasuta, Solid State Ionics 132 (2000) 261.
[5] J.H. Wang, M. Liu, Electrochem. Commun. 9 (2007) 2212.
[6] Y.H. Huang, R.I. Dass, Z.-L. Xing, J.B. Goodenough, Science 312 (2006) 254–257.
[7] S.-E. Hou, J.A. Alonso, J.B. Goodenough, J. Power Sources 195 (1) (2010) 280–284.
[8] A. Aguadero, J.A. Alonso, D. Perez-Coll, C. de la Calle, M.T. Fernandez-Diaz, J.B. Goodenough, Chem. Mater. 22 (2010) 789–798.
[9] S.-E Hou, J.A. Alonso, S. Rajasekhara, M.J. Martinez-Lope, M.T. Fernandez-Diaz, J.B. Goodenough, Chem. Mater. 22 (2010) 1071.
[10] B.L. Chamberland, P.S. Danielson, J. Solid State Chem. 3 (1971) 243–247.
[11] J. Zhou, N.S. Xu, S.Z. Deng, J. Chen, J.C. She, Z.L. Wang, Adv. Mater. 15 (2003) 1835.
[12] B.D. Gaulin, J.N. Reimers, T.E. Mason, J.E. Greedan, Z. Tun, Phys. Rev. Lett. 69 (1992) 3244.
[13] B.C. Zhao, Y.P. Sun, S.B. Zhang, W.H. Song, J.M. Dai, J. Appl. Phys. 102 (2007) 10.1063.
[14] J.A. Alonso, M.J. Martínez-Lope, A. Aguadero, L. Daza, Prog. Solid State Chem. 36 (2008) 134–150.
[15] H.M. Rietveld, J. Appl. Crystallogr. 2 (1969) 65–71.
[16] J. Rodríguez-Carvajal, Physica B 192 (1993) 55–69.
[17] R.D. Shannon, Acta Crystallogr. A32 (1976) 751–767.
[18] R.B. Macquart, B.J. Kennedy, M. Avdeev, J. Solid State Chem. 183 (2010) 250–255.
[19] M. Retuerto, J.A. Alonso, M.J. Martínez-Lope, J.L. Martínez, M. García-Hernández, Appl. Phys. Lett. 85 (2004) 266.
[20] P. Huang, A. Horky, A. Petric, J. Am. Ceram. Soc. 82 (9) (1999) 2402.
[21] K.N. Kim, B.K. Kim, J.W. Son, J. Kim, H.W. Lee, J.H. Lee, J. Moon, Solid State Ionics 177 (2006) 2155.
[22] Y. Lin, S.A. Barnett, Electrochem. Solid-State Lett. 9 (6) (2006) A285.
[23] Z. Bi, Y. Dong, M. Cheng, B. Yi, J. Power Sources 161 (2006) 34.
[24] X. Zhang, S. Ohara, R. Manic, K. Mukai, T. Fukui, H. Yoshida, M. Nishimura, T. Inagaki, K. Miura, J. Power Sources 83 (1999) 170.